Journal of Molecular Structure 973 (2010) 173–179

Contents lists available at ScienceDirect

Journal of Molecular Structure

journal homepage: www.elsevier.com/locate/molstruc

An ester derivative of the drug gabapentin: pH dependent crystal stability

Vânia André [a], M. Matilde Marques [a], M.F. Minas da Piedade [a,b], M. Teresa Duarte [a,*]

[a] Centro de Química Estrutural, Departamento de Engenharia Química e Biológica, Instituto Superior Técnico, Av. Rovisco Pais 1, 1049-001 Lisbon, Portugal
[b] Departamento de Química e Bioquímica, Faculdade de Ciências da Universidade de Lisboa, Av. Prof. Gama Pinto, 1649-003 Lisbon, Portugal

ARTICLE INFO

Article history:
Received 18 February 2010
Received in revised form 18 March 2010
Accepted 29 March 2010
Available online 2 April 2010

Keywords:
Gabapentin
Crystal engineering
Prodrug
Hydrogen bonding
pH dependence

ABSTRACT

Gabapentin solutions with different pHs were prepared and slow crystallization was allowed to occur. Different crystalline forms were obtained at pHs up to 7, whereas alkaline media (pH 9) gave rise to an amorphous product. A new crystal structure of an ethyl ester derivative, obtained at pH 2 under Fischer esterification conditions, is described herein. Esterification blocked the supramolecular interactions typically observed through the carboxyl group of gabapentin, which resulted in a dramatic change in the solid-state structure. As it is known, this change could have a marked influence on the physiological absorption characteristics of the drug, which supports the search for ester-based gabapentin prodrugs as a means of improving the limited bioavailability of the drug.

1. Introduction

The search for new crystal forms has become one of the major issues in modern solid-state chemistry, materials chemistry and pharmaceutical science. When these new crystal forms involve active pharmaceutical ingredients (API) the potential for new discoveries, innovation and market protections, as well as intellectual property issues, can be of the most importance leading to a tremendous evolution in studies on multicomponent crystal forms in the last several years [1–19].

Gabapentin is a structural analog of γ-aminobutyric acid (GABA) with demonstrated therapeutic use in epilepsy, neuropathic pain, restless legs syndrome, anxiety disorders, hot flashes and numerous other indications. The drug is currently marketed as an adjunct therapy for partial seizures in adults with epilepsy and for management of postherpetic neuralgia [20].

Gabapentin exists as a zwitterion in three anhydrous polymorphic forms [21–23]: forms II, III and IV, with II being the most stable and IV the least stable. Furthermore, two monohydrate [24–26], two polymorphic chloride hemihydrate [27,28] and a hemisulfate hemihydrate (isomorphous of a gabapentin hydrochloride hemihydrate form [27]) forms [29] have also been reported. Coordination complexes of this API with Cu and Zn [30] as well as multicomponent crystal forms (cocrystals and salts) involving gabapentin with different carboxylic acids were recently disclosed [23,31–33].

Gabapentin itself is highly soluble but has limited and variable bioavailability, probably due to its dependence on a low-capacity amino-acid transporter expressed in a limited region of the upper small intestine. Moreover, gabapentin absorption saturates at clinical doses, which results in dose-dependent pharmacokinetics and considerable interpatient variability. Therefore, the development of prodrugs of this API, with better absorption properties and capable of releasing the parent drug *via* enzymatic hydrolysis, has recently been receiving much attention [20,32,34].

In the pursuit of new crystal forms of gabapentin, a pH-dependence study of this API was undertaken, not only to check for its stability but mainly to look for new derivatives with potential therapeutic applications. Having the same functional groups as an aminoacid, gabapentin is especially dependent on the pH of the environment. For that reason, simple changes in the acidity conditions may lead to different final products and the elucidation of these differences was the goal of the present study. At low pH a new ester derivative involving the breaking and forming of covalent bonds was disclosed, and in milder conditions hydrogen bonds breaking and forming are responsible for the formation of the known chloride hemihydrate form. A comparison study between both forms is discussed herein. None of these forms are stable at high temperatures and structural transformations are detected by XRPD.

2. Results and discussion

Following our expectations, gabapentin is pH-sensitive, forming both conventional covalent bonds, which gave rise to the ethyl es-

* Corresponding author. Tel.: +351 218419282.
E-mail address: teresa.duarte@ist.utl.pt (M.T. Duarte).

0022-2860/$ - see front matter © 2010 Elsevier B.V. All rights reserved.
doi:10.1016/j.molstruc.2010.03.067

ter and undergoing supramolecular bonding, forming the chloride hemihydrate, in our experimental conditions (Scheme 1). An amorphous product is obtained whenever basic conditions are employed.

Not unexpectedly, the ester, **1**, is only obtained at low pH (pH 2), concomitantly with the chloride hemihydrate, **2**. The powder diffraction pattern of the bulk mixture of **1** and **2** (Fig. 1) reveals that the chloride hemihydrate is present in a higher proportion than the ester. Under the experimental conditions, gabapentin is expected to undergo Fischer esterification (Scheme 2) with a low yield, consistent with this acid-catalyzed equilibrium reaction.

All the other acidic experimental conditions led to the formation of pure crystalline **2** (pH 3 and 3.5) (Fig. 2), avoiding all the covalent bond breaking and forming. At even milder pH (pH 5–7), different polymorphic forms of gabapentin (Fig. 3) were isolated depending on the cooling rate of the solutions: the slowest cooling rate always yielded form III while faster coolings constantly resulted in form II. Both proved to be stable for at least 1 month in laboratory conditions. At higher pH values, only amorphous product was obtained.

The molecular and crystal structures of both **1** and **2** will next be discussed and compared here, as they were both obtained concomitantly. We have also performed thermal studies on this mixture and they will be illustrated and discussed.

2.1. Molecular and crystal structures

This section presents a detailed analysis of the molecular and crystal structure of the ester derivative from gabapentin (see Fig. 4), followed by a comparative description of the chloride hemihydrate form obtained concomitantly and a general discussion on conformation details. The most recent disclosed polymorph of the chloride hemihydrates is not discussed herein as its presence is not detected in any of our samples. Detailed geometric parameters of the hydrogen bonds are given in Table 1.

The location in the electron density map and the perfect refinement of three hydrogen atoms around the N atoms in the crystal structure of **1** demonstrated that the ester derivative is protonated in the amine moiety and Cl^- acts as a counterion. The C–O distances in the ester moiety (1.343 Å and 1.203 Å) clearly indicate the existence of single and double bonds.

At the supramolecular level, all the hydrogen bonds established in this structure involve the Cl anions and there are no direct interactions between the ester ammonium cations. In a view along *b*, the gabapentin ester aligns in two anti-parallel chains connected through the anion by two hydrogen bonds: $N_1–H_{02}\cdots Cl^-$ and $N_1–H_{03}\cdots Cl^-$, the molecules being equally oriented (Fig. 5a). The remaining $N_1–H_{01}\cdots Cl^-$ bonding is used to connect this 2D pattern with similar ones in parallel planes along *b*, thus forming a layered structure of ester cations along *a*.

Also worth noticing is the pattern observed along c, in which the supramolecular assemblies form a 3-dimensional channel bearing the N and the Cl ions in the vertices. The hydrogens of

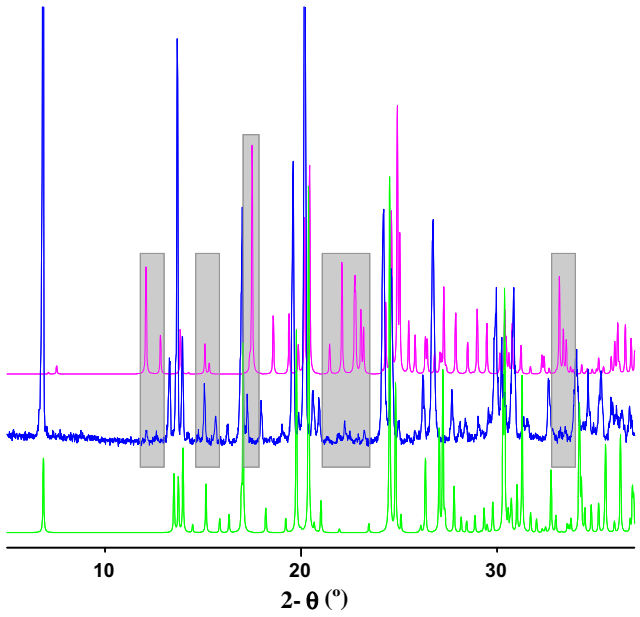

Fig. 1. Theoretical powder diffraction patterns obtained from single-crystal data of **1** (top) and **2** (bottom), at 150 K, are represented for identification of the phases. Experimental powder diffraction pattern (middle) obtained from the bulk, corresponding to the mixture of gabapentin ethyl ester (**1**) and gabapentin chloride hemi-hydrate (**2**) at room temperature. The main peaks that allow the identification of **1** in the bulk are highlighted in grey.

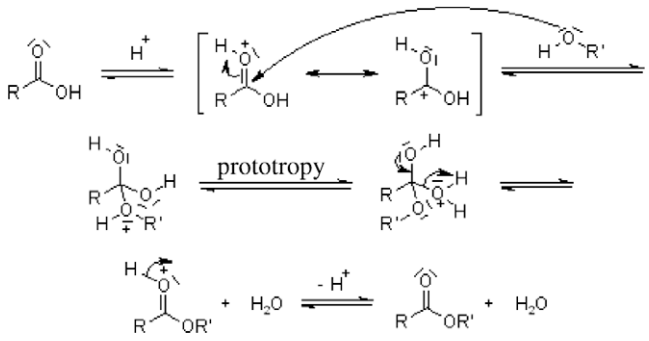

Scheme 2. Generic mechanism of the Fischer esterification.

the ammonium group are aligned along the faces of this cube (Fig. 5b). This motif is repeated along *a* and *b*, giving rise to a cage-like 3-dimensional array. We should stress that this crystal packing does not involve any oxygen atom, thus deactivating the acceptor ability of both the carbonyl and the ether functions, presumably due to steric constraints.

Similarly to what is observed in **1**, in **2** gabapentin is also protonated in the amine moiety. This was ascertained both by the

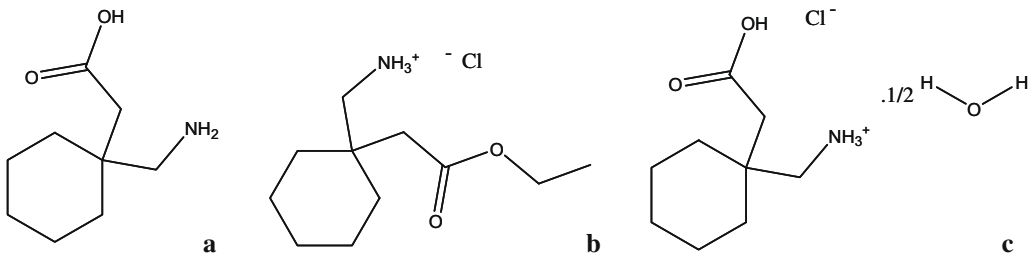

Scheme 1. Structure of (a) gabapentin, (b) gabapentin ethyl ester chloride, **1** (c) gabapentin chloride hemihydrate, **2**.

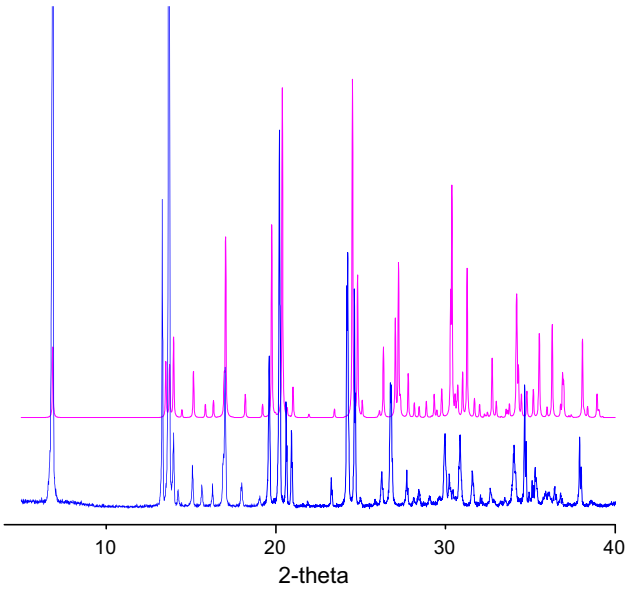

Fig. 2. Experimental powder diffraction pattern (bottom) obtained from the synthesis at pH 3.5 and theoretical powder diffraction patterns obtained from single-crystal data of **2** (top), at 150 K.

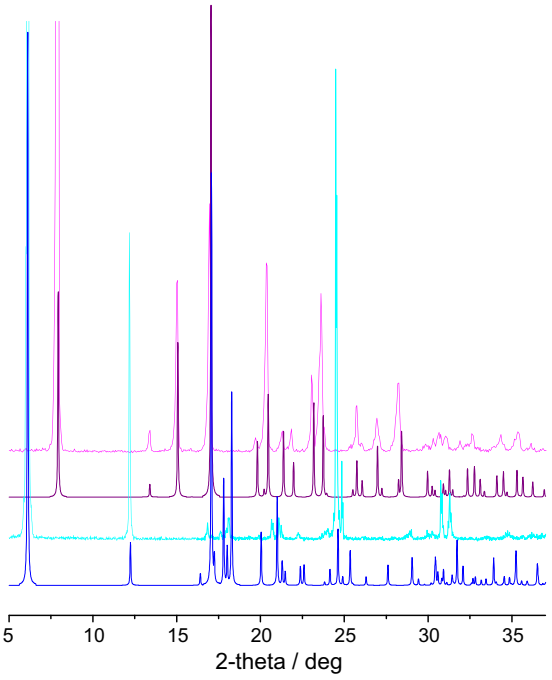

Fig. 3. Experimental powder diffraction patterns obtained from the synthesis at pH 5–7 and theoretical powder diffraction patterns obtained from single-crystal data of gabapentin forms II and III, at 150 K.

location of the hydrogen atoms in the amine and carboxylic moieties and by the C–O distances (1.325 Å and 1.210 Å). In the gabapentin cations, an intramolecular hydrogen-bond (N^+–H···O) is established between the ammonium and the carboxylic moieties (Fig. 6a).

In **2**, gabapentin cations interact directly with each other through N–H···O hydrogen bonds thus forming a dimer based in $R_2^2(4)$ synthon, also involving the intramolecular bond. These dimers are reinforced by intermolecular interactions with the chlorine anions (Fig. 6a).

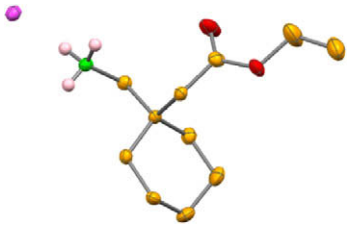

Fig. 4. Molecular diagram of **1**, determined at 150 K. Ellipsoids are set at 50% probability and calculated hydrogen atoms were omitted for clarity. Colour code: yellow – carbon; green – nitrogen; red – oxygen; magenta – chlorine; light pink – hydrogens. (For interpretation of the references to colour in this figure legend, the reader is referred to the web version of this article.)

Table 1
List of hydrogen bonds for **1** and **2**.

Structure	Sym. Op.	D–H···A	d(D–H) (Å)	d(H···A) (Å)	d(D···A) (Å)	(DĤA) (deg)
	1/2−*x*, 3/2−*y*, *z*	$N_1H_{01}\cdots Cl$	0.85(3)	2.41(3)	3.243(3)	166(2)
1	*x*, *y*, *z*	$N_1H_{02}\cdots Cl$	0.93(3)	2.22(3)	3.156(3)	177(2)
	1/2−*x*, *y*, 1/2 + *z*	$N_1H_{03}\cdots Cl$	0.92(3)	2.24(3)	3.151(3)	168(2)
	x, *y*, *z*	$N_1H_1\cdots O3$	0.90(2)	2.03(2)	2.915(2)	171(2)
	x, *y*, *z*	$N_1H_2\cdots O1$	0.88(2)	2.05(2)	2.760(2)	137(2)
2	1−*x*, 1−*y*, −*z*	$N_1H_2\cdots O1$	0.88(2)	2.53(2)	2.883(2)	104(2)
	x, *y*, *z*	$N_1H_3\cdots Cl$	0.87(3)	2.37(2)	3.231(2)	171(2)
	1−*x*, 1−*y*,−*z*	$O_2H_8\cdots C1$	0.87(2)	2.14(3)	3.008(2)	177(2)
	x, −1 + *y*, *z*	$O_3H_{19}\cdots C1$	0.79(2)	2.42(2)	3.183(1)	163(2)

The water molecules act as spacers along *c* connecting the dimeric motifs, thus obtaining two chains of cations. In these chains the cyclohexane rings of consecutive gabapentin cations are rotated by 46.9(4)° (Fig. 6b). The chlorine anions besides supporting the dimers using N^+–H···Cl^- charge-assisted hydrogen bonds also play a part when obtaining the anti-parallel chains as they act as acceptors for the water and the hydroxyl function of the carboxylic moiety. The role of water is very important in the 3D array obtained as they interact directly with two gabapentin cations related by an inversion centre, acting as hydrogen acceptors (N^+H···O). Its role is further reinforced as they also work as donors for the chlorine anions.

The crystal structure of **1** is distinct from any of the reported gabapentin forms: both the synthons formed and the type of interactions is different, as the packing of **1** is dominated by charged-assisted N^+–H···Cl^- hydrogen bonds.

In **2**, the presence of the intramolecular hydrogen bond and the formation of the $R_2^2(4)$ synthon resemble what is observed in polymorphic form IV of gabapentin, the only polymorph that shows an intramolecular interaction. The charged-assisted N–H···O interactions present in **2** are also the only type of interactions observed in the three polymorphic forms of gabapentin.

Gabapentin shows a clear predisposition to form chains not only in both forms detailed above but also in the three known polymorphic forms [QIMKIG01, QIMKIG02 and QIMKIG03] [21–23] (Fig. 7).

The three known polymorphic forms of gabapentin are conformational polymorphs. Trying to rationalize the conformation of the structures presented here we compared their solid-state conformation with the above mentioned polymorphic forms. For this comparison, the conformation and substituent positioning are defined relatively to the cyclohexane backbone.

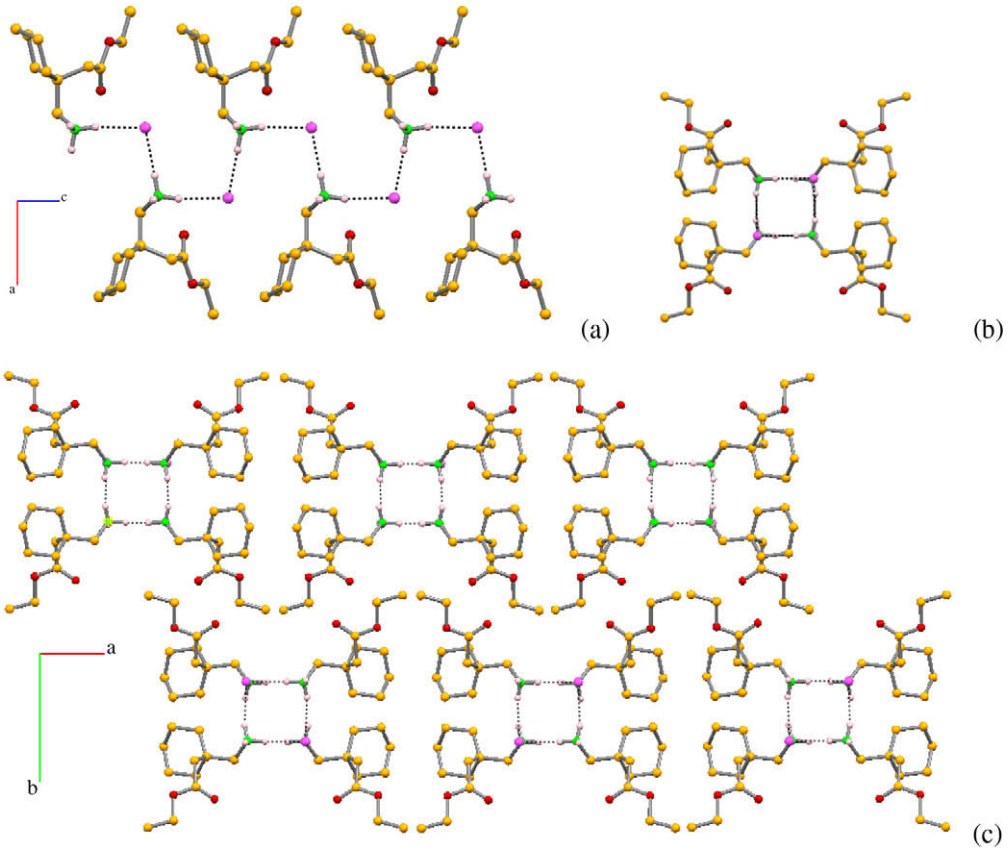

Fig. 5. Intermolecular interactions in the gabapentin ethyl ester structure (a) view along *b* of the anti-parallel chains connected through the Cl anions; (b) detailed view of the supramolecular channel motif; (c) cage-like array seen along *c*.

In both **1** and **2** the ring adopts a chair conformation (mean $\theta = 4.7(2)^\circ$) [35], in resemblance with what is observed in the known polymorphic forms of gabapentin. In the new crystal forms reported herein, the aminomethyl group is in an equatorial position, and the carboxethyl group in the axial position. This relative positioning of the substituent groups is similar to the one observed in gabapentin form IV; in the other two polymorphic forms the relative positions are reversed (see Fig. 8).

3. Thermal studies

In an attempt to further characterize the concomitantly crystallized **1** and **2**, thermal studies were performed and are discussed here.

The thermogram of the mixture **1** and **2** (Fig. 9) showed two consecutive endothermic peaks, the first at approximately 110 °C and the second around 126 °C. Comparing with the thermogram obtained with the pure hemihydrate form, the peak at higher temperature corresponds to the melting of the latter; the lower temperature peak is due to melting of the new ester form.

The smaller contribution from the ester observed in the thermogram is a consequence of its low percentage in the bulk material, as already mentioned.

The irregular baseline in the DSC plot led us to perform powder diffraction studies for the bulk mixture of **1** and **2** at different temperatures (Fig. 10). This study reveals some structural changes at 60 °C and major changes at 100 °C. Changes were investigated, but no conclusions were reached about which new structure(s)

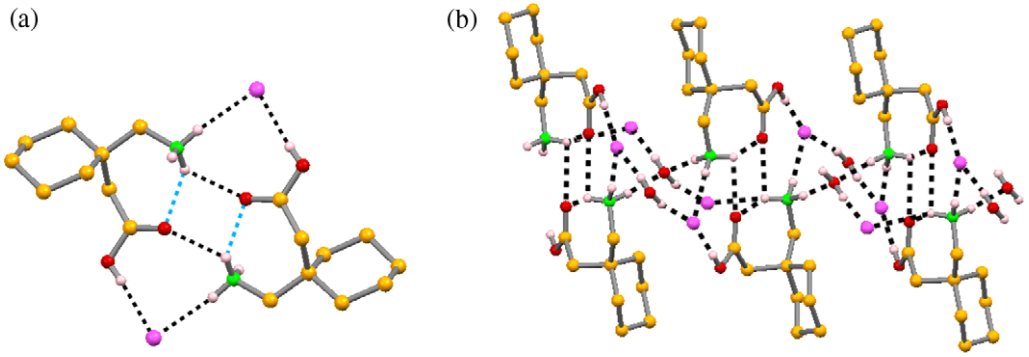

Fig. 6. (a) Dimeric motif showing the $R_2^2(4)$ synthon, using intra and intermolecular hydrogen bonds, represented in blue, and reinforced by interactions with the anions; (b) chains of gabapentin cations held together by chloride anions and water molecules, the O atom residing on an inversion centre. (For interpretation of the references to colour in this figure legend, the reader is referred to the web version of this article.)

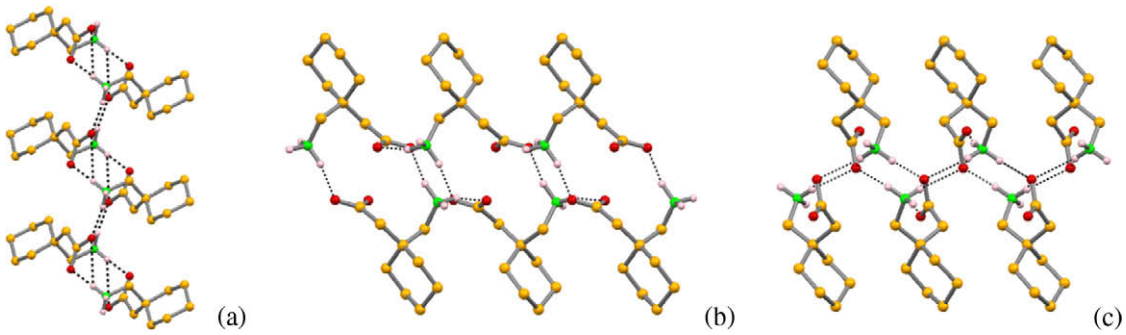

Fig. 7. Chain motifs of gabapentin forms: (a) II, (b) III and (c) IV.

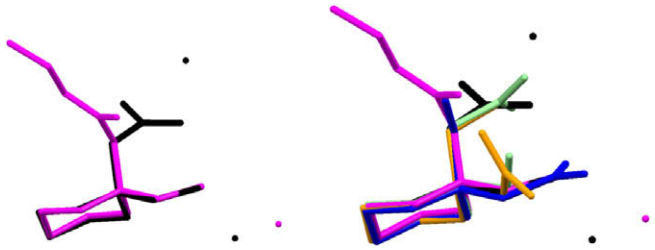

Fig. 8. Molecular structures of **1** (magenta), **2** (black) and gabapentin polymorphic forms II (blue), III (orange) and IV (green). (For interpretation of the references to colour in this figure legend, the reader is referred to the web version of this article.)

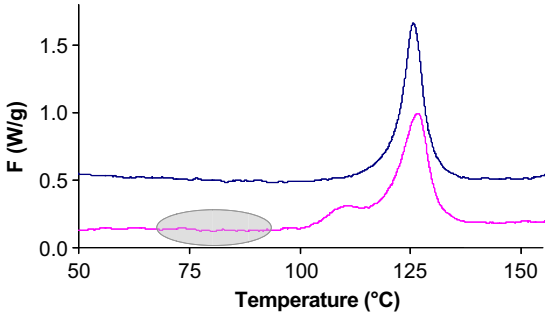

Fig. 9. Thermogram obtained from the mixture of **1** and **2** (bottom), at a heating rate of 5 °C/min, in a closed aluminium capsule, with a sample of 7.6 mg. (ΔH_{global} = 101.315 J/g) compared with a thermogram of pure **2** (top) obtained in similar conditions (ΔH_{global} = 98.758 J/g).

was(were) being formed. These transformations are not immediately reversible, as the diffractogram collected after cooling to room temperature is similar to the diffractogram collected at 100 °C. Nonetheless, we observed that the form produced at high temperature is not stable and is converted into **2** after a few months on the shelf.

One hypothesis for the explanation of the appearance of this new form would be the transformation of both **1** and **2** into gabapentin–lactam [23], but this was discarded by comparing the experimental diffractogram obtained after heating and the theoretical diffractogram of the known form of the lactam [refcode AWUWOE] [27] (Fig. 10).

4. Experimental

4.1. Synthesis

All reagents were acquired from Sigma and used as received. pH measurements were performed using a pH electrode Hanna HI 9025. All the solid products were analysed by XRPD.

4.1.1. Crystallization of gabapentin at pH 2

A solution of gabapentin form II (0.1436 g, 0.839 mmol) in a blend of ethanol (4 mL) and water (0.1 mL) was heated at boiling temperature for 5 min. The final pH of this solution was about 7 and a few drops of HCl 37% were added until the solution reached pH2.

The solution was left to crystallize at room temperature, by slow evaporation of the solvents. After 4 days, two different types of colourless crystals could be identified under the microscope: thick needles (gabapentin ethyl ester [ethyl (1-(aminomethyl)cyclohexyl)acetate], **1**) and plate-like (gabapentin chloride hemihydrate, **2**). Both these forms grew concomitantly in the bulk, as proven by XRPD.

4.1.2. Crystallization of gabapentin at pH 3 and 3.5

Two solutions of gabapentin form II (0.5854 g, 3.419 mmol and 0.5855 g, 3.419 mmol) in a blend of ethanol (3 mL) and water (2 mL) were prepared and heated at boiling temperature for 30 min. The pH of these solutions was approximately 7. Drops of HCl 37% were added to both solutions until pH 3 was reached in one and pH 3.5 in the other. The solutions were left to crystallize at room temperature, by slow evaporation of the solvents. After 1 day, crystals of gabapentin chloride hemihydrate, **2**, formed in both preparations.

4.1.3. Crystallization of gabapentin at pH 5–7

Several crystallizations of gabapentin were performed in the pH range from 5 to 7, using water and ethanol as solvents and conditions similar to those described in the other experiments reported herein. These experiments always yielded gabapentin polymorphic form II. Within this pH range, and maintaining similar experimental conditions but cooling the solution more slowly by using manual cooling steps of 0.5 °C/min in the hot-plate, form III could also be isolated.

4.1.4. Crystallization of gabapentin at pH 9

Gabapentin form II (0.3670 g, 2.1430 mmol) was dissolved in 2.5 mL of ethanol and heated at boiling temperature for 30 min. After heating, the solution was filtered for removal of the undissolved material. The pH of this solution was 7 and a few drops of NaOH solution (0.5 M) were added until pH 9 was reached. The solution was left to crystallize at room temperature, by slow evaporation of the solvents. After 2 days an amorphous material was observed.

4.2. Crystal structure determination

Single-crystal X-ray structures were determined for **1** and **2**. Both crystal structures were determined at 150 K on a Bruker AXS-KAPPA APEX II diffractometer with graphite-monochromated

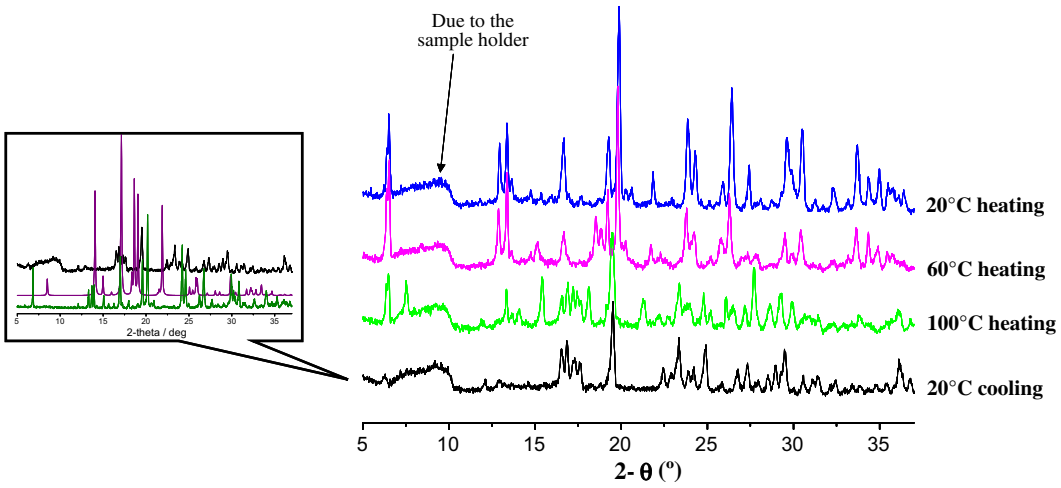

Fig. 10. Powder diffraction patterns obtained from a mixture of a **1** and **2**, at different temperatures (right) and comparison of the final product obtained after heating (top left) with gabapentin–lactam (middle left) and the transformation into **2** after a few months on the shelf (bottom left).

radiation (Mo Kα, λ = 0.71069 Å). The X-ray generator was operated at 50 kV and 30 mA. All data were corrected for Lorentzian, polarization and absorption effects using SAINT [36] and SADABS [37] programs. SIR97 [38] was used for structure solution and SHELXL-97 [39] was used for full matrix least-squares refinement on F^2. All non-hydrogen atoms were refined anisotropically. H_{NH} atoms were located from a difference Fourier map and their positional coordinates and isotropical parameters were refined. H_{CH} atoms were added in calculated positions and refined riding on their C atoms. MERCURY 2.2 [40] was used for packing diagrams.

Table 2 summarizes the crystallographic data for **1** and **2**.

4.3. X-ray powder diffraction analysis at room temperature

Powder data were collected in a D8 Advance Bruker AXS θ–2θ diffractometer, with a copper radiation and a secondary monochromator, operating at 40 kV and 30 mA. Data were acquired in the range 5° < 2θ < 38°, using a 0.016 step size and 1.5 s/step.

The program PowderCell 2.4 [41] was used for calculation of the X-ray powder patterns. The correspondence between the bulk material and the structures obtained by single crystals was verified by comparing calculated and observed powder diffraction patterns.

Table 2
Summary of crystallographic data for crystal structures **1** and **2**.

	1	**2**
Chemical formula	$C_{11}H_{22}NO_2C1$	$C_{18}H_{38}N_2O_5C1_2$
M_r	235.75	433.4
Temperature (K)	150(2)	150(2)
Wavelength (Å)	0.71069	0.71069
Morphology, colour	Thick needle, colourless	Plate, colourless
Crystal size (mm)	0 18 × 0.10 × 0.04	0.20 × 0.14 × 0.02
Crystal system	Orthorhombic	Monoclinic
Space group	Pccn	C2/c
a (Å)	14.632(2)	27.746(7)
b (Å)	23.460(3)	6.540(1)
c (Å)	7.460(4)	13.173(3)
β (deg)	90	111.766(1)
V (Å^3)	2560.8(15)	2219.9(8)
Z	8	4
Calculated density (mg m^{-3})	1.223	1.297
Absorption coefficient (mm^{-1})	0.282	0.322
θ min (deg)	2.73	3.21
θ max (deg)	25.34	26.44
Reflections collected/unique	15,233/2341	13,674/2263
R_{int}	0.0962	0.0634
GoF	0.85	1.08
Threshold expression	>2σ(I)	>2σ(I)
R_1 (obsd)	0.0373	0.0329
wR_2 (all)	0.0744	0.045

4.4. X-ray powder diffraction analysis at different temperatures

In order to check for structural changes of the bulk mixture of **1** and **2** with temperature, powder diffraction patterns were acquired at different temperatures.

The data were collected in a RIGAKU D300 diffractometer, with copper radiation and a secondary monochromator, operating at 40 kV and 30 mA. Data were collected from 2θ 5 to 38°, using a 0.02 step size and 1 s/step. Different diffractograms were collected at 20 °C, 60 °C and 100 °C. After the samples returned to room temperature, new diffractograms at 20 °C were collected to evaluate the reversibility of the transformations occurred.

4.5. DSC measurements

The thermal behavior of the mixture of **1** and **2** obtained was investigated by measuring the enthalpy change on a Setaram DSC121 calorimeter. Crystals (7.6 mg) were placed on a closed aluminium pan and were analysed from 40 to 200 °C, using an empty pan as the reference. The heating rate was 5 °C/min and argon gas was used for purging.

5. Conclusions

Gabapentin is very sensitive to pH variations in solution, which may lead to the breaking and forming of either covalent or hydrogen bonds allowing the discovery of new crystal forms of this API.

The esterification presented herein induced a dramatic change in the solid-state characteristics of the gabapentin scaffold, blocking the supramolecular interactions associated with the carboxylic acid moiety, to such an extent that the carboxyethyl group was even inactive as a hydrogen bond acceptor. The typical charge-assisted N–H···O hydrogen-bonds observed in the forms of gabapentin are totally replaced by N–H···Cl interactions in the ethyl ether disclosed herein, once the functional groups have changed and the formation of the salt is preferred. This alteration resulted in a less compact packing that could have an effect upon the rate of disso-

lution and membrane permeability of the drug under physiological conditions. Given the significance of kinetic solubility in drug absorption phenomena [42], our results substantiate the search for ester prodrugs of gabapentin as a means of achieving improved bioavailability.

Acknowledgements

The authors acknowledge funding of the Project POCI/QUI/58791/2004 and PhD Grant SFRH/BD/40474/2007 by Fundação para a Ciência e a Tecnologia.

References

[1] C.B. Aakeroy, M.E. Fasulo, J. Desper, Molecular Pharmaceutics 4 (2007) 317–322.
[2] S.L. Childs, G.P. Stahly, A. Park, Molecular Pharmaceutics 4 (2007) 323–338.
[3] N. Takata, K. Shiraki, R. Takano, Y. Hayashi, K. Terada, Crystal Growth & Design 8 (2008) 3032–3037.
[4] M.B. Hickey, M.L. Peterson, L.A. Scoppettuolo, S.L. Morrisette, A. Vetter, H. Guzman, J.F. Remenar, Z. Zhang, M.D. Tawa, S. Haley, M.J. Zaworotko, O. Almarsson, European Journal of Pharmaceutics and Biopharmaceutics 67 (2007) 112–119.
[5] J.F. Remenar, M.L. Peterson, P.W. Stephens, Z. Zhang, Y. Zimenkov, M.B. Hickey, Molecular Pharmaceutics 4 (2007) 386–400.
[6] A.V. Trask, J. van de Streek, W.D.S. Motherwell, W. Jones, Crystal Growth & Design 5 (2005) 2233–2241.
[7] A.V. Trask, W.D.S. Motherwell, W. Jones, International Journal of Pharmaceutics 320 (2006) 114–123.
[8] A.M. Chen, M.E. Ellison, A. Peresypkin, R.M. Wenslow, N. Variankaval, C.G. Savarin, T.K. Natishan, D.J. Mathre, P.G. Dormer, D.H. Euler, R.G. Ball, Z.X. Ye, Y.L. Wang, I. Santos, Chemical Communications (2007) 419–421.
[9] K.M. Anderson, M.R. Probert, C.N. Whiteley, A.M. Rowland, A.E. Goeta, J.W. Steed, Crystal Growth & Design 9 (2009) 1082–1087.
[10] D.J. Berry, C.C. Seaton, W. Clegg, R.W. Harrington, S.J. Coles, P.N. Horton, M.B. Hursthouse, R. Storey, W. Jones, T. Friscic, N. Blagden, Crystal Growth & Design 8 (2008) 1697–1712.
[11] C.C. Sun, H. Hou, Crystal Growth & Design 8 (2008) 1575–1579.
[12] A.D. Bond, Crystengcomm 9 (2007) 833–834.
[13] B.R. Sreekanth, P. Vishweshwar, K. Vyas, Chemical Communications (2007) 2375–2377.
[14] M. Rafilovich, J. Bernstein, M.B. Hickey, M. Tauber, Crystal Growth & Design 7 (2007) 1777–1782.
[15] G.G.Z. Zhang, R.F. Henry, T.B. Borchardt, X.C. Lou, Journal of Pharmaceutical Sciences 96 (2007) 990–995.
[16] A. Jayasankar, D.J. Good, N. Rodriguez-Hornedo, Molecular Pharmaceutics 4 (2007) 360–372.
[17] W.W. Porter, S.C. Elie, A.J. Matzger, Crystal Growth & Design 8 (2008) 14–16.
[18] M.T. Kirchner, D. Das, R. Boese, Crystal Growth & Design 8 (2008) 763–765.
[19] D.K. Bucar, R.F. Henry, X.C. Lou, T.B. Borchardt, G.G.Z. Zhang, Chemical Communications (2007) 525–527.
[20] K.C. Cundy, T. Annamalai, L. Bu, J. De Vera, J. Estrela, W. Luo, P. Shirsat, A. Torneros, F.M. Yao, J. Zou, R.W. Barrett, M.A. Gallop, Journal of Pharmacology and Experimental Therapeutics 311 (2004) 324–333.
[21] J.A. Ibers, Acta Crystallographica Section C – Crystal Structure Communications 57 (2001) 641–643.
[22] H.A. Reece, D.C. Levendis, Acta Crystallographica Section C – Crystal Structure Communications 64 (2008) O105–O108.
[23] D. Braga, F. Grepioni, L. Maini, K. Rubini, M. Polito, R. Brescello, L. Cotarca, M.T. Duarte, V. Andre, M.F.M. Piedade, New Journal of Chemistry 32 (2008) 1788–1795.
[24] P.G. Vasudev, S. Aravinda, K. Ananda, S.D. Veena, K. Nagarajan, N. Shamala, P. Balaram, Chemical Biology & Drug Design 73 (2009) 83–96.
[25] D.E. Butler, B.J. Greenman, New crystalline gabapentin mono: hydrate used in prepn. of pure anhydrous gabapentin and in treatment of epilepsy, fainting attacks, hypokinesia and cranial traumas. WARNER-LAMBERT CO and WARNER LAMBERT CO. [EP340677-A2; AU8932678-A; DK8902126-A; FI8902067-A; JP2011546-A; US4894476-A; US4960931-A; CA1306755-C; EP340677-B1; DE68912819-E; ES2061774-T3; IE62958-B; JP2619951-B2; DK200200056-A; DK175127-B; DK175400-B].
[26] L.J. Bosch, M.D.C. Onrubia Miguel, L.E. Pagans, M.C. Onrubia Miguel, L.J. Bosch, M.M.C. Onrubia, L.E. Pagans, New crystalline gabapentin mono: hydrate. MEDICHEMIE, S. A. [WO200064857-A; EP1174418-A; WO200064857-A1; AU200035592-A; EP1174418-A1; ES2164527-A1; HU200200741-A2; US6528682-B1; ES2164527-B1; EP1174418-B1; DE60007734-E; ES2213571-T3; IN200101052-P2; IL145920-A].
[27] K. Ananda, S. Aravinda, P.G. Vasudev, K.M.P. Raja, H. Sivaramakrishnan, K. Nagarajan, N. Shamala, P. Balaram, Current Science 85 (2003) 1002–1011.
[28] J.P. Jasinski, R.J. Butcher, H.S. Yathirajan, L. Mallesha, K.N. Mohana, B. Narayana, Journal of Chemical Crystallography 39 (2009) 777–780.
[29] S. Chava, S.R. Gorantla, V.S.K. Indukuri, V.S.K. Indukurl, C. Satyanarayana, G.S. Ramanjaneyulu, I.V. Kumar, Preparation of Gabapentin Form-II for the treatment of cerebral diseases e.g. epilepsy, involves neutralization of Gabapentin hemisulfate hemihydrate solution with base at higher temperature, followed by cooling. MATRIX LAB LTD, CHAVA S, and GORANTLA. [WO2004093780-A2; EP1615875-A2; US2006235079-A1; US7439387-B2].
[30] D. Braga, F. Grepioni, L. Maini, R. Brescello, L. Cotarca, Crystengcomm 10 (2008) 469–471.
[31] M. Wenger, J. Bernstein, Crystal Growth & Design 8 (2008) 1595–1598.
[32] H.T. Wu, G. Kaur, G.L. Griffiths, Tetrahedron Letters 50 (2009) 2100–2102.
[33] L.S. Reddy, S.J. Bethune, J.W. Kampf, N. Rodriguez-Hornedo, Crystal Growth & Design 9 (2009) 378–385.
[34] P. Revill, J. Bolos, N. Serradell, M. Bayes, Drugs of the Future 31 (2006) 771–777.
[35] J.C.A. Boeyens, Journal of Crystal and Molecular Structure 8 (1978) 317–320.
[36] Bruker AXS: SAINT+, release 6.22. Bruker Analytical Systems: Madison, WI, 2005.
[37] Bruker AXS:SADABS. Bruker Analytical Systems: Madison, WI, 2005.
[38] A. Altomare, M.C. Burla, M. Camalli, G.L. Cascarano, C. Giacovazzo, A. Guagliardi, A.G.G. Moliterni, G. Polidori, R. Spagna, Journal of Applied Crystallography 32 (1999) 115–119.
[39] G.M. Sheldrick, Acta Crystallographica Section A 64 (2008) 112–122.
[40] C.F. Macrae, I.J. Bruno, J.A. Chisholm, P.R. Edgington, P. McCabe, E. Pidcock, L. Rodriguez-Monge, R. Taylor, J. van de Streek, P.A. Wood, Journal of Applied Crystallography 41 (2008) 466–470.
[41] G. Nolze, W. Kraus, Powder Diffraction 13 (1998) 256–259.
[42] E.H. Kerns, L. Di, Drug-like Properties: Concepts, Structure Design and Methods, Academic Press, 2008.